engineering proceedings

MDPI

Proceeding Paper

Exploration of Fluidic Thrust Vectoring Control on a Dynamic Test Rig: Computational and Experimental Analysis †

Ahsan Tanveer [1,*] and Sarvat Mushtaq Ahmad [2,3]

[1] Department of Mechanical & Aerospace Engineering, Institute of Avionics & Aeronautics, Air University, Islamabad 44000, Pakistan
[2] Control & Instrumentation Engineering Department, King Fahd University of Petroleum and Minerals, Dhahran 31261, Saudi Arabia; sarvat.ahmad@kfupm.edu.sa
[3] Interdisciplinary Research Center for Intelligent Manufacturing and Robotics, King Fahd University of Petroleum and Minerals, Dhahran 31261, Saudi Arabia
* Correspondence: ahsantanveer3883@gmail.com or ahsan.tanveer@mail.au.edu.pk
† Presented at the 4th International Electronic Conference on Applied Sciences, 27 October–10 November 2023; Available online: https://asec2023.sciforum.net/.

Abstract: Fluidic thrust vectoring (FTV) control is a cutting-edge method used to manipulate the motion of an unmanned air vehicle when traditional control surfaces like elevators are not available. The primary purpose of employing FTV is to make the aircraft less detectable. This research centers around the exploration of the co-flow variation of the FTV concept. In this approach, a secondary jet with a significant velocity is injected into the boundary layer of the primary jet. As a consequence, the primary jet is diverted, leading to the formation of a pitch moment. Numerical simulations were conducted to analyze different ratios of secondary and primary jet velocities, providing valuable insights into the effectiveness of the proposed technique. The test rig, designed with a pitch-constraint dynamic setup, utilized electric ducted fans to generate primary and secondary flows. At 19 m/s primary velocity, the experimental testing shows a maximum vertical force of 0.4 N, producing a deflection of 25°, which is deemed adequate for thrust vectoring. This research builds upon the authors' previous work on characterizing a static co-flow FTV rig. The comparison between the computational fluid dynamics analyses and the experimental results demonstrates agreement in the behavior of the vectored jet. This validation further strengthens the findings presented in this paper.

Keywords: unmanned aerial vehicle; fluidic thrust vectoring control; co-flow FTV; Coanda effect; computational fluid dynamics

Citation: Tanveer, A.; Ahmad, S.M. Exploration of Fluidic Thrust Vectoring Control on a Dynamic Test Rig: Computational and Experimental Analysis. *Eng. Proc.* **2023**, *52*, 0. https://doi.org/

Academic Editor: Firstname Lastname

Published:

1. Introduction

When unmanned air vehicles (UAVs) were initially introduced a couple of decades ago, their primary objective was focused on surveillance and information gathering tasks, particularly for missions that were deemed monotonous, hazardous, or unsuitable for manned flights. However, as technology rapidly advanced and mission requirements became more complex, stealth UAVs began to emerge. Stealth attributes in UAVs can be achieved by employing unique alloys within a traditional airframe, or through creative design of the UAV body and novel methods for controlling airflow. This article primarily focuses on the latter strategy.

Mechanical thrust vectoring (MTV) has been employed in various military aircraft, such as McDonnell Douglas AV-8B Harrier II [1], F-35 Lightning II [2], and X-15 [3], to reduce radar cross-section by eliminating the need for traditional control surfaces. MTV is additionally employed to augment the effectiveness of the traditional control surfaces [4]. In recent times, there has been significant interest in a novel flow control concept known as fluidic thrust vectoring (FTV) [5]. FTV is founded on the principle of redirecting the primary jet through the introduction of a secondary jet. This concept has garnered significant interest

because of its benefits, which encompass minimal or absent movable components and a swifter dynamic reaction when contrasted with MTV [6].

Fluidic thrust vectoring (FTV) concepts encompass various techniques, including counter-flow, co-flow, throat shifting, and shock-vector control. While FTV has garnered substantial interest in the realm of supersonic aircrafts, this research places its emphasis on the practical implementation of FTV in subsonic UAVs. Previous studies have demonstrated the co-flow FTV concept on prototype vehicles, showcasing closed-loop control [7,8]. However, the existing literature predominantly focuses on FTV utilization for supersonic jets, while limited research is dedicated to sub-sonic UAVs, which is the primary focus of this work. Additionally, supersonic studies typically involve convergent-divergent nozzles, while convergent nozzles are more suitable for sub-sonic studies. Therefore, an autonomous inquiry is imperative to establish foundational subsonic co-flow FTV models and subsequently subject them to experimental validation.

The primary aim of this study is to execute a fundamental investigation, showcasing the effectiveness of the subsonic co-flow FTV concept for a dynamic UAV test rig. The investigation scrutinizes two critical factors: the velocity of the primary jet and the velocity of the secondary jet, both of which wield an impact on the efficacy of fluidic thrust vectoring. Thorough computational fluid dynamics (CFD) simulations are carried out to ascertain the ideal jet velocities that ensure proficient pitch control for the UAV. A comparison is drawn between the CFD outcomes and the empirical observations derived from the experiments.

The remaining sections of the paper are organized as follows: Section 2 introduces the co-flow thrust vectoring concept. Section 3 presents the CFD numerical simulations. The experimental test setup is described in Section 4. CFD and experimental results are presented in Section 5. Finally, Section 6 concludes the paper.

2. The Concept of Co-Flow FTV

Within traditional thrust vectoring techniques, a secondary jet is incorporated into the primary jet's flow, thereby adjusting its trajectory and managing pitch movement. Specifically, in the co-flow strategy, momentum is supplemented to the primary jet, resulting in meticulous control over the primary exhaust orientation [9]. The concept of co-flow is depicted in Figure 1.

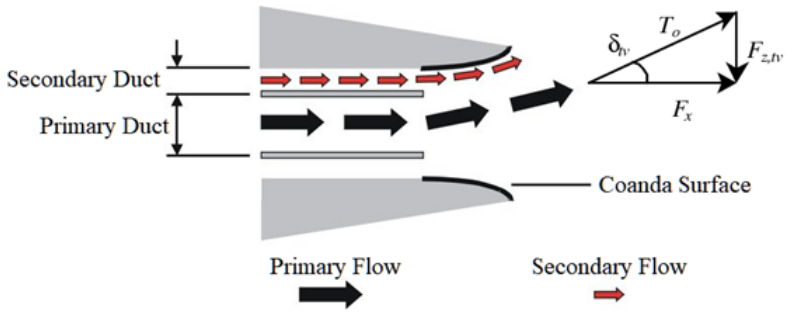

Figure 1. An Illustration of the Co-Flow Thrust Vectoring principle [10].

By examining the geometry presented in Figure 1, it can be observed that when the secondary jet adheres to the upper Coanda surface, it generates an imbalanced force on the surface. This results in the generation of a net thrust vector force (F_z) in the downward direction, as depicted in Figure 1. Consequently, this force creates a sufficient pitching moment around the UAV's center of gravity, enabling the vehicle to achieve trim during flight. The estimation of the thrust deflection angle ($\theta_{t.v.}$) can therefore be determined as:

$$\theta_{t.v.} = tan^{-1}(\frac{F_z}{F_x}) \quad (1)$$

The forces F_x and F_z denote the force components along the x and z-axes, respectively. These forces are derivable by combining primary and secondary flow attributes, which include velocities and flow rates.

2.1. Nozzle Configuration

Figure 2 showcases the geometry of the co-flow nozzle and its associated design variables. The rectangular nozzle employed in this study is of the convergent type, purposely developed to investigate the concept of co-flow FTV.

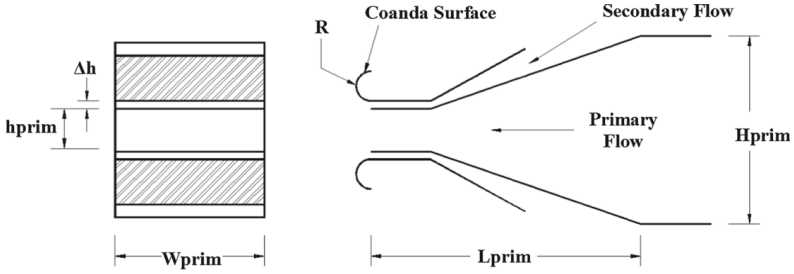

Figure 2. Schematic illustrating geometry of the co-flow FTV nozzle [11].

3. The Computational Approach

The accurate and reliable solution of the Navier-Stokes equations is essential in Computational Fluid Dynamics (CFD) analysis. In this study, the Solidworks Flow Simulation, a commercial tool known for its advanced solver technology, is employed. Solidworks utilizes a unique finite-volume method (FVM) to discretize the Navier-Stokes equations, ensuring efficient convergence and robust results.

To facilitate the design of the experimental demonstrator FTV test rig, a computational analysis using Solidworks was performed, focusing on 2D flow. The nozzle CAD geometry, also created in Solidworks, was imported into Flow Simulation solver. A three-dimensional structured meshing scheme comprising of rectangular (grade 3) elements was constructed at the nozzle exit geometry. As the solver employed a wall boundary condition, the number of elements was considerably higher in the vicinity of the Coanda surfaces and nozzle walls compared to the outer domain. CFD simulations were conducted to gather velocity data and flow orientation, which were then compared with experimental data for validation.

The performance of the nozzle and the thrust vectoring angle were determined using the post-processing capabilities of Solidworks Flow Simulation package. Additionally, flow contours were visualized and the flow velocity was calculated using the post-processing tool.

4. Experimental Setup

In this study, an experimental setup was developed and designed, as illustrated in Figure 3. The FTV nozzle was made out of galvanized sheets, with specific dimensions and ratios: a Coanda radius of 25 mm, a primary height of 70 mm, and a secondary exit gap height of 1.2 mm. The experimental setup comprises the FTV nozzle linked to the main primary duct.

To generate the primary and secondary streams, a 3000 kv Electronic Ducted Fan (EDF) and a 2600 kv EDF were utilized, correspondingly. Control of primary and secondary jet flows is accomplished through motor controllers dedicated to the EDFs, and flow velocities are gauged via a Pitot tube. The arrangement of Coanda surfaces and the primary and secondary nozzles encourages the tangential movement of the secondary jet along the curved Coanda surfaces, effectively enabling fluidic thrust vectoring via co-flow. To render the flow visible, tufts are employed.

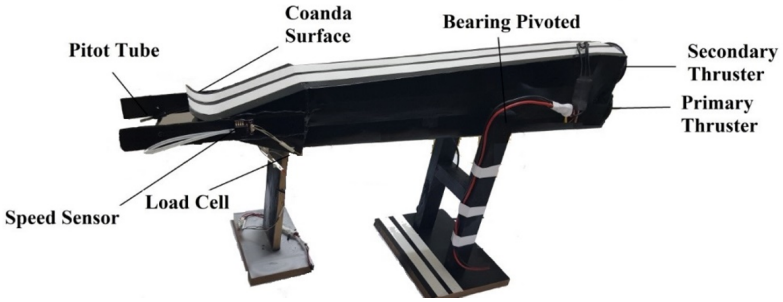

Figure 3. Co-flow experimental test rig.

4.1. Experimentation

Throughout the experiments, the primary exit velocity remained constant, while the secondary velocity was varied from 0 to 40 m/s. Velocity measurements were taken with a Pitot tube, and the primary jet deflection angle was read manually from a protractor aligned with the thrust axis. This process was repeated for various secondary flow velocities, with corresponding deflection angles recorded. Images were captured at 30 frames per second (fps) for each secondary exit velocity to validate the experimental deflection angle readings of the primary jet.

5. Results

This section focuses on the analysis of CFD results, including a comparison with experimental findings. Furthermore, the study explores flow separation phenomena within the computational domain, particularly at low Reynolds numbers.

5.1. Computational Results

To gain an understanding of the dynamic behavior of the FTV nozzle, several CFD experiments were conducted. The system was subjected to varying secondary velocities, and the corresponding primary jet deflections were recorded under steady-state conditions. Figure 4 illustrates the computational results obtained for different secondary exit velocities. It can be observed that as the primary velocity increases, the inactive or dead zone decreases, indicating a faster response. Subsequently, a series of experiments were conducted for a specific ratio of primary to secondary velocities, and the findings from these experiments are presented in the following sections.

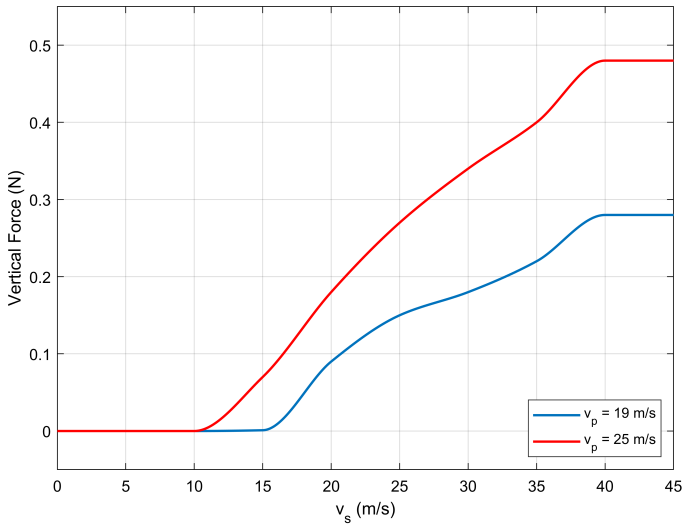

Figure 4. Vertical force versus secondary flow velocity.

5.2. Comparison of Computational and Experimental Results

The CFD simulations were conducted under operating conditions that closely matched those used in the experimental study. Specifically, the simulations and experiments were performed for a secondary velocity of 0–40 m/s. In terms of qualitative flow analysis, velocity streamlines were extracted from the CFD simulations (Figure 5a,c). These streamlines were then compared with the images of the vectored jets captured using a high-definition camera during the experiments.

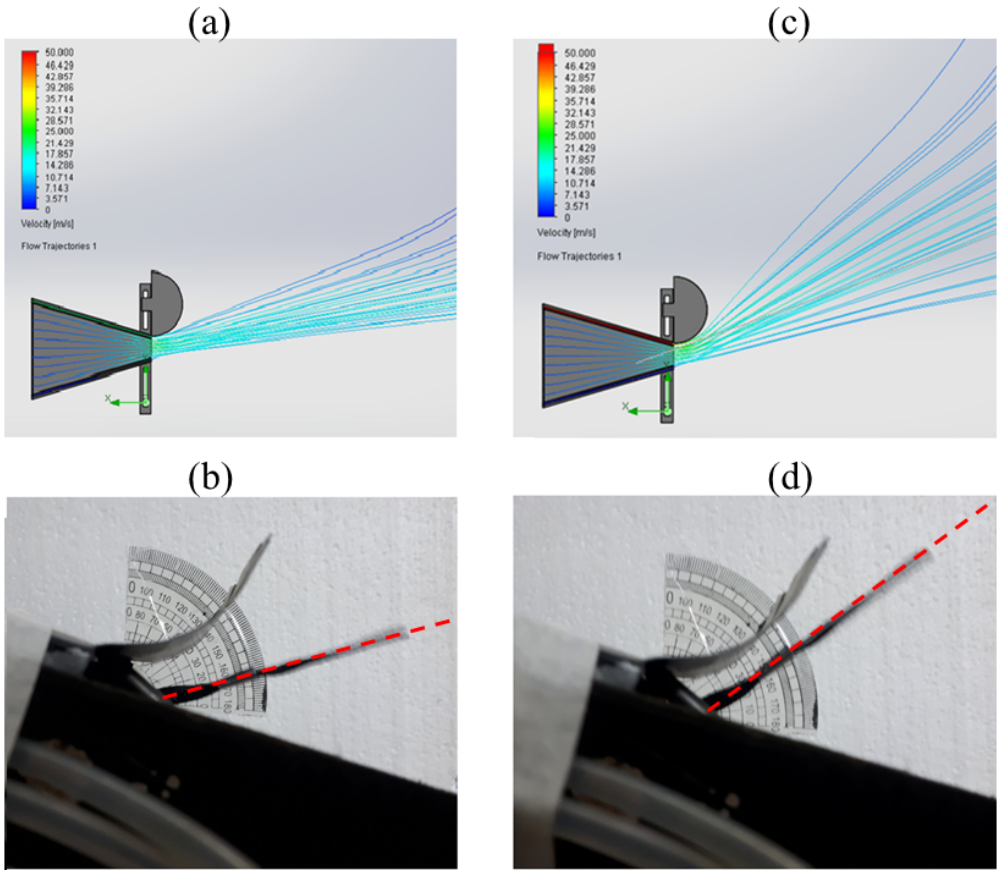

Figure 5. Flow visualization for: (**a**) CFD at v_s/v_p = 1.32. (**b**) Experimental at v_s/v_p = 1.32. (**c**) CFD at v_s/v_p = 1.6. (**d**) Experimental at v_s/v_p = 1.6.

Figure 5 presents selected test cases with varying primary and secondary velocities. It is clear that the CFD images, which depict velocity streamlines on the symmetry plane, closely resemble those captured from the experimental setup. The predicted thrust vectoring angles obtained through CFD simulations align closely with the angles measured in the experiments. For the two cases illustrated, the percentage difference between the CFD and experimental FTV angles is approximately 7% and 6% respectively.

The pitching moment (M), representing the moment produced about the c.g. of the aircraft, for different values of primary velocity, is depicted in Figure 6a. The figure also depicts the correlation between changes in secondary jet velocity and the resulting pitching moment in the experimental case. As expected, an increase in primary velocity leads to a corresponding increase in moment. For values of secondary velocity beyond 40 m/s, the experimental results indicate moment stagnation. In the case of secondary velocity up to 10 m/s no pitching moment is generated by the exhaust jet.

Furthermore, the entire deflection plot (Figure 6b) can be divided into three distinct regimes: the dead zone, control region, and saturation region, based on the varying slopes of the curves in these regions. In the dead zone (for v_s < 10 m/s), thrust vectoring is not possible as the curves have a lower slope compared to the control region (for 10 m/s < v_s <

35 m/s), where the curves are much steeper. There is a marginal increase in slope in the saturation region ($v_s > 35$ m/s), where effective thrust vectoring is not feasible. Therefore, from an aircraft control perspective, the control region is of interest, as efficient thrust vectoring can be achieved in this region.

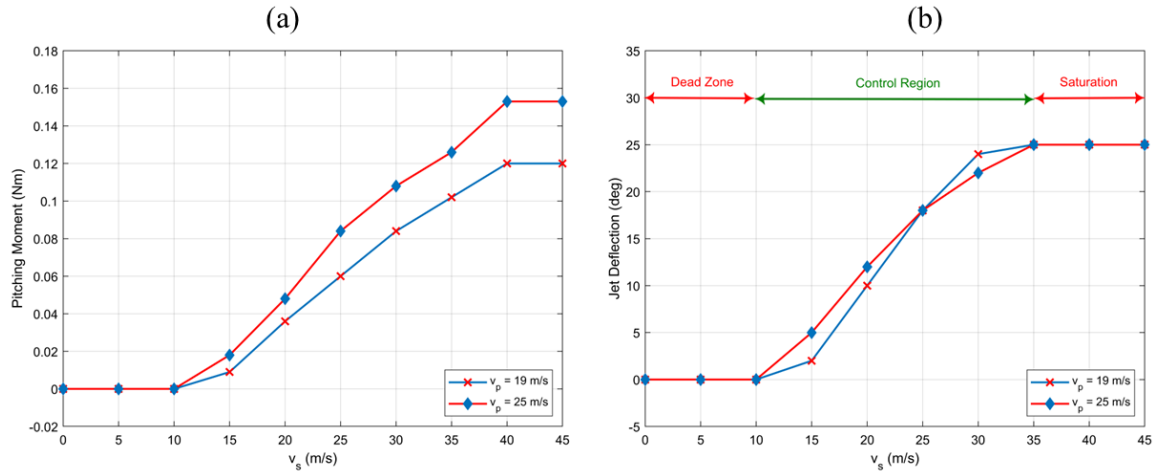

Figure 6. Experimental response: (**a**) Pitching moment versus secondary flow velocity. (**b**) Jet deflection versus secondary flow velocity.

6. Conclusions

The present study aimed to investigate the co-flow fluidic thrust vectoring concept through the development of a foundational operational test rig. The outcomes of the computational fluid dynamics (CFD) simulations indicated that a higher v_s/v_p ratio confers advantages in achieving effective thrust vectoring. Conversely, simulations illustrated that decreasing the primary velocity leads to an enlarged inactive or dead zone, which induces a delay in the responsiveness of the vectored jet. Notably, both the experimental and computational findings corroborated the same pattern. The computational simulations accurately predicted the trend for the various cases studied. Both simulations and experiments indicated the presence of a dead zone at lower secondary velocities, where no thrust vectoring occurred. At higher secondary velocities, saturation occurred, resulting in minimal or no further increase in the angle of deflection. The region of interest for UAV trimming, referred to as the control region, lies between these limits and involves an investigation that warrants further exploration.

Author Contributions: Conceptualization, A.T. and S.M.A.; methodology, A.T.; software, A.T.; validation A.T. and S.M.A.; formal analysis, A.T.; investigation, A.T.; resources, S.M.A.; data curation, A.T.; writing—original draft preparation, A.T.; writing—review and editing, S.M.A.; visualization, A.T.; supervision, S.M.A.; project administration, S.M.A. All authors have read and agreed to the published version of the manuscript.

Funding: This research received no external funding.

Institutional Review Board Statement:

Informed Consent Statement:

Data Availability Statement:

Conflicts of Interest: The authors declare no conflict of interest.

References

1. Postlethwaite, I.; Bates, D.G. Robust integrated flight and propulsion controller for the Harrier aircraft. *J. Guid. Control Dyn.* **1999**, *22*, 286–290.
2. Wiegand, C. F-35 air vehicle technology overview. In Proceedings of the 2018 Aviation Technology, Integration, and Operations Conference, Atlanta, GA, USA, 25–29 June 2018; p. 3368.

3. Sahbon, N.; Jacewicz, M.; Lichota, P.; Strzelecka, K. Path-Following Control for Thrust-Vectored Hypersonic Aircraft. *Energies* **2023**, *16*, 2501.
4. Anderson, C.; Giuliano, V.; Wing, D.; Anderson, C.; Giuliano, V.; Wing, D. Investigation of hybrid fluidic/mechanical thrust vectoring for fixed-exit exhaust nozzles. In Proceedings of the 33rd Joint Propulsion Conference and Exhibit, Seattle, WA, USA, 6–9 July 1997; p. 3148.
5. Afridi, S.; Khan, T.A.; Shah, S.I.A.; Shams, T.A.; Mohiuddin, K.; Kukulka, D.J. Techniques of Fluidic Thrust Vectoring in Jet Engine Nozzles: A Review. *Energies* **2023**, *16*, 5721.
6. Das, A.K.; Acharyya, K.; Mankodi, T.K.; Saha, U.K. Fluidic Thrust Vector Control of Aerospace Vehicles: State-of-the-Art Review and Future Prospects. *J. Fluids Eng.* **2023**, *145*, 080801.
7. Capello, E.; Ferrero, A.; Marsilio, R.; Ferlauto, M. CFD-based Fluidic Thrust Vectoring model for fighter aircraft. In Proceedings of the AIAA Propulsion and Energy 2019 Forum, Indianapolis, IN, USA, 19–22 August 2019; p. 4311.
8. Wu, L.; Li, H.; Li, Y.; Li, C. Position tracking control of tailsitter VTOL UAV with bounded thrust-vectoring propulsion system. *IEEE Access* **2019**, *7*, 137054–137064.
9. Shi, N.X.; Gu, Y.S.; Zhou, Y.H.; Wang, L.X.; Feng, C.; Li, L.K. Mechanism of hysteresis and uncontrolled deflection in jet vectoring control based on Coanda effect. *Phys. Fluids* **2022**, *34*.
10. Tanveer, A.; Ahmad, S.M. Mathematical Modelling and Fluidic Thrust Vectoring Control of a Delta Wing UAV. *Aerospace* **2023**, *10*, 563.
11. Ahmad, S.; Siddique, S.; Yousaf, M.; Tariq, M.; Khan, M.; Alam, M. Computational and experimental investigation of fluidic thrust vectoring actuator. *J. Braz. Soc. Mech. Sci. Eng.* **2018**, *40*, 315.